

Direct Imaging of a Novel Silicon Surface Reconstruction

J. M. Gibson, M. L. McDonald, and F. C. Unterwald

AT&T Bell Laboratories, Murray Hill, New Jersey 07974

(Received 14 August 1985)

Silicon surface reconstructions are directly observed in profile by high-resolution transmission-electron microscopy. Low-energy surface facets are formed at edges by *in situ* annealing of a $\langle 110 \rangle$ thin specimen at an ambient pressure of 10^{-9} Torr. As well as $\langle 111 \rangle$, $\langle 100 \rangle$, and $\langle 110 \rangle$ reconstructed surfaces, extensive areas of flat $\langle 113 \rangle$ surface are found. By inspection of high-resolution images from the $\langle 113 \rangle$ surface a model involving one dimer per surface (1×1) unit cell is proposed, suggesting that low-energy surfaces need not be confined to high-symmetry orientations.

PACS numbers: 68.20.+t, 61.16.Di

Electron microscopy has been used in the transmission geometry to study clean silicon surfaces by diffraction and imaging.^{1,2} Images taken with surface superlattice reflections in dark field have been reported by Takayanagi³ and theoretical studies of diffraction and imaging have been published by Spence⁴ and Krivanek and Wood.⁵ However, to date, no high-resolution bright-field images of the silicon surface reconstructions have been published. For the Au $\langle 110 \rangle$ surface such images have been formed in the profile geometry,⁶ although under poorly controlled surface conditions.

In this Letter we report preliminary observations of silicon surface reconstructions obtained by high-resolution transmission electron microscopy in an instrument modified for an ultrahigh-vacuum specimen environment with *in situ* specimen-heating facilities. Both profile and plan-view geometries have been used, the former proving most fruitful for straightforward observation of surface structure. A specimen-preparation method is used which allows the profile observation of a large number of surface orientations, over reasonably extended regions (typically $10\,000 \times 200 \text{ \AA}^2$). Low-energy surface orientations can be identified and their reconstructions observed. Although both the $\langle 111 \rangle$ and $\langle 100 \rangle$ surfaces and their reconstructions are seen, a surprising observation is that flat areas of $\langle 113 \rangle$ surface occur frequently, always exhibiting a dramatic (1×1) "sawtooth" structure. A simple model of this surface is proposed which fits the data quite well. The dangling-bond density on this surface is comparable with that for $\langle 100 \rangle$ and other high-index orientations. Indeed, it would be interesting to study the properties of large-area surfaces cut in the $\langle 113 \rangle$ orientation. Perhaps the horizons of surface scientists are too often confined to high-symmetry orientations. Our technique for identifying low-energy surfaces should be applicable to many materials.

Specimens were prepared for profile observation from $\langle 110 \rangle$ 10- Ω -cm *p*-type silicon wafers by chemical thinning in a mixture of 3HF/5HNO₃. For plan-

view observation some samples were similarly prepared from $\langle 111 \rangle$ wafers. After thinning almost to perforation the sample surfaces were cleaned with a modified Shiraki chemical procedure.⁷ Specimens were kept in deionized water until insertion in the microscope vacuum system. The specimen region of the electron microscope is differentially pumped to a pressure of $< 2 \times 10^{-8}$ Torr and a considerable vacuum improvement in the vicinity of the specimen is achieved by He cryoshielding. The specimen is heated resistively *in situ* to $> 1000^\circ\text{C}$. The details of the microscope and heating stage will be published elsewhere. After *in situ* annealing at $\approx 1200^\circ\text{C}$ of plan-view $\langle 111 \rangle$ specimens we observe the (7×7) reconstruction which persists for over 30 min on cooling to room temperature. This is an indication of the cleanliness of our vacuum system and the immediate specimen environment. Figure 1(a) shows a transmission-electron diffraction pattern and 1(b) a bright-field phase-contrast image showing the (7×7) superstructure. Intensities in the diffraction pattern are in qualitative agreement with previous observations.^{1,2} Surface imaging in the transmission geometry, such as Fig. 1(b), is productive but it can be difficult to form suitably thin, clean specimen areas and reconstruction usually occurs on both surfaces. The area viewed in Fig. 1(b) is heavily stepped, so that fringes shift across the image.

After annealing at $> 1000^\circ\text{C}$ the thin edges of $\langle 110 \rangle$ -oriented specimens facet onto low-energy surfaces, primarily $\langle 111 \rangle$, $\langle 100 \rangle$, $\langle 110 \rangle$, and $\langle 113 \rangle$. Figure 2 shows profile images in the $\langle 110 \rangle$ direction of the $\langle 100 \rangle$ and $\langle 113 \rangle$ surfaces taken at about 400°C . (Specimen temperature is often held in excess of room temperature to improve cleanliness.) The $\langle 100 \rangle$ surface shows the well-known (2×1) reconstruction.⁸ Detailed interpretation of $\langle 100 \rangle$ images will be presented in a later publication. The $\langle 113 \rangle$ surfaces exhibit a dramatic "sawtooth" structure indicative of regions of higher and lower projected potential. Although it can be difficult to estimate the specimen thickness near the edge, it appears that the

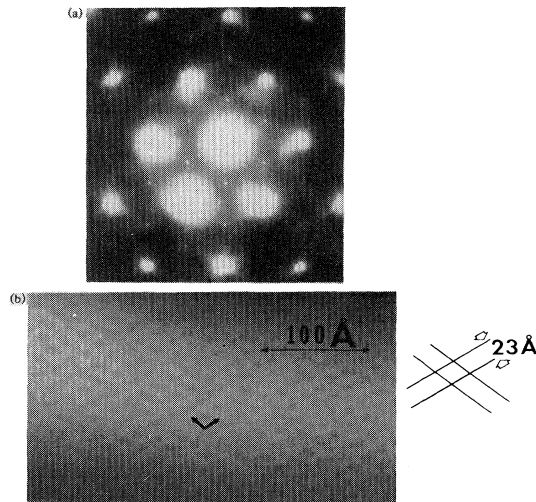


FIG. 1. (a) Transmission-electron diffraction pattern and (b) high-resolution bright-field image of the Si $\langle 111 \rangle$ (7×7) surface reconstruction in plan-view geometry from a $\langle 111 \rangle$ thin specimen. Only the $\frac{1}{7}$ th-order diffraction spots contribute to the image, giving rise to sets of 23-Å-spacing fringes. Dark areas represent regions of higher projected potential in this image.

white regions in image 2(b) correspond to regions of high projected potential (atoms). Only by this assumption can reasonable agreement between simulations and experiment be obtained. Simulated images

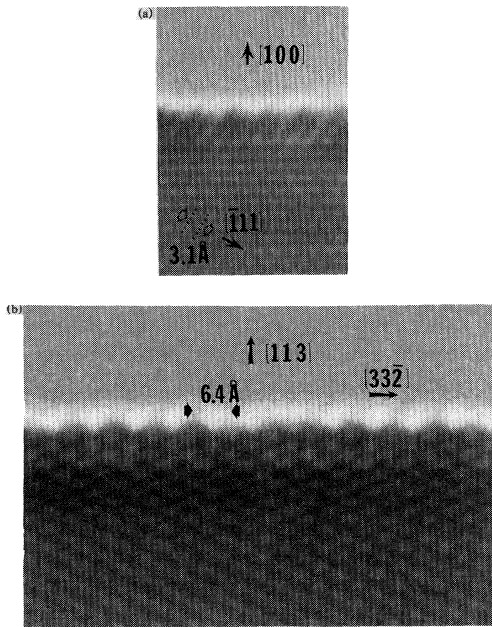


FIG. 2. Profile images at high resolution from surface facets at the edge of a $\langle 110 \rangle$ Si specimen showing (a) the $\langle 100 \rangle$ (2×1) surface and (b) the $\langle 113 \rangle$ (1×1) surface.

were obtained with the multislice algorithm.⁹ Figure 3 is a projection of a proposed model for the $\langle 113 \rangle$ reconstructed surface. The period of this reconstruction is (1×1) . (It should be stressed that the images give confirmation of this period only in one direction: $\langle 33\bar{2} \rangle$.) One dimer is introduced per unit cell to minimize the number of dangling bonds. The simulated image agrees well with experiment; however, until a more quantitative analysis is carried out, we cannot exclude other possible atomic models. The dimer bond length used in the calculation is 15% longer than the equilibrium length and atomic displacements are

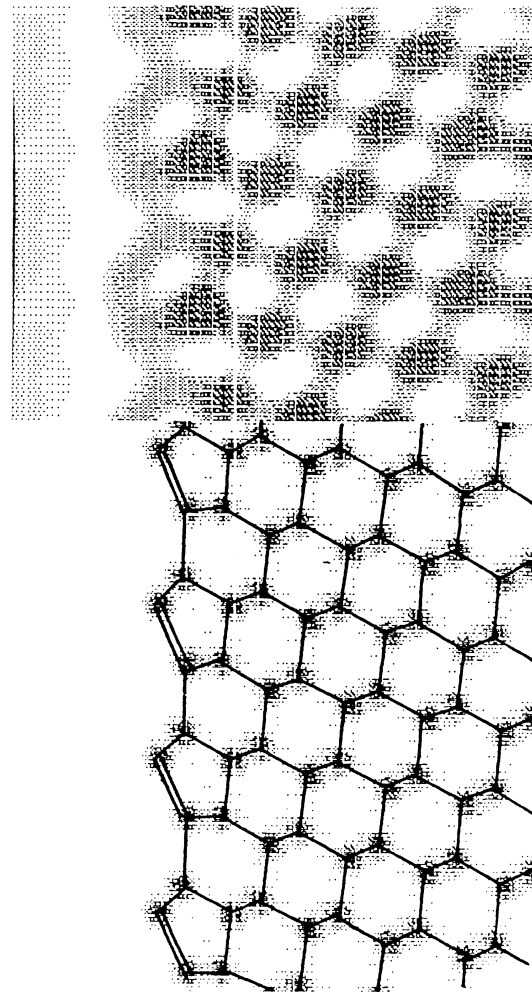


FIG. 3. Model and simulated image of the reconstructed Si $\langle 113 \rangle$ surface involving dimerization of one pair of atoms per unit cell (marked by double lines). Parameters used in the image simulation were defocus, -950 Å; specimen thickness, 60 Å; and others appropriate to the JEOL 200CX instrument. There is good agreement between the experimental image of Fig. 2 and this calculated image, although images are not very sensitive to dimer bond length under these conditions (accuracy $\pm 10\%$).

15%. Although the image detail is sensitive to detailed atomic positions, uncertainty over imaging parameters prevents direct measurement of atom positions with great accuracy.¹⁰ Image simulations taking into account possible misalignment and careful experimental work are necessary for determination of more detailed structure.

The $\langle 113 \rangle$ crystallographic plane is known as the habit plane of certain defects in silicon¹¹ and inspection of its structure shows that it could be a relatively low-energy surface. The simple model proposed for the $\langle 113 \rangle$ (1×1) surface is sensible in view of the known existence of similar dimerization on the Si $\langle 100 \rangle$ and $\langle 111 \rangle$ surfaces. The density of dangling bonds per unit surface area with this model is $4.8 \times 10^{14} \text{ cm}^{-2}$. This is comparable with the low-energy $\langle 111 \rangle$ and $\langle 100 \rangle$ (2×1) surfaces. As such it is an interesting example of the possibility that low-energy surfaces, particularly in the presence of reconstruction, need not be of highest bulk symmetry. The same arguments may apply to interfaces and grain boundaries.

The profile geometry is well-suited to examination of surface structure, particularly for "deep" surface reconstructions. Surfaces, although limited in dimension in one direction, are considerably extended parallel to the specimen edge. The fact that we have observed (111) (7×7) and (100) (2×1) reconstructions in this mode confirms that the line tension effects at surface boundaries in its limited direction do not seriously interfere with reconstruction, for silicon at least. Obviously it would be appropriate to study large-area $\langle 113 \rangle$ surfaces by plan-view transmission-electron microscopy and conventional surface-science techniques. Detailed studies of the $\langle 111 \rangle$ and $\langle 100 \rangle$ surface structures will be published at a later date. Both plan-view and profile geometries are, in fact, complementary in surface studies with transmission-electron microscopy.

In conclusion, we demonstrate the first high-resolution profile images of silicon surface reconstructions. The technique of annealing a thin specimen and observing surface faceting at the edges allows the iden-

tification of the lowest-energy surfaces. We find unexpectedly that the $\langle 113 \rangle$ surface is favored and exhibits a strong, apparently (1×1) , reconstruction. A dimer model of this reconstruction is proposed that agrees well with the high-resolution images and contains a low density of dangling bonds, without excessive atomic displacements. It appears that low-energy surfaces need not be confined to high-symmetry orientations and that this technique is well suited for identifying favorable surface orientations and their reconstructions.

We acknowledge the invaluable assistance of the JEOL company, particularly Mr. Y. Naruse, in the design of the UHV instrument and Mr. A. Insano for his skilled machining.

¹K. Takayanagi, Y. Tanashiro, M. Takahashi, and S. Takahashi, *J. Vac. Sci. Technol. A* **3**, 1502 (1985).

²P. M. Petroff and R. J. Wilson, *Phys. Rev. Lett.* **51**, 199 (1983).

³K. Takayanagi, *J. Microsc. (Oxford)* **136**, 287 (1984).

⁴J. C. H. Spence, *Ultramicroscopy* **11**, 117 (1983).

⁵O. L. Krivanek and G. J. Wood, in *Proceedings of the Forty-Third Annual Meeting of the Electron Microscopy Society of America*, edited by G. W. Bailey (San Francisco Press, San Francisco, 1985), p. 262.

⁶L. D. Marks, *Phys. Rev. Lett.* **51**, 1000 (1983).

⁷A. Ishizaka, K. Nakagawa, and Y. Shiraki, in collected papers of the Second International Symposium on Molecular Beam Epitaxy and Related Clean Surface Techniques, 27–30 August 1982 (unpublished), p. 183

⁸R. E. Schlier and H. E. Farnsworth, *J. Chem. Phys.* **30**, 917 (1959).

⁹A 128×128 array size was used with 355 beams and an objective aperture radius 0.4 \AA^{-1} , spherical aberration coefficient $C_s = 1.2 \text{ mm}$, and electron wavelength 0.025 \AA . A supercell size of $6.4 \times 33.3 \text{ \AA}^2$ was used. The algorithm is described by J. M. Cowley, in *Diffraction Physics* (North-Holland, New York, 1981).

¹⁰J. M. Gibson, *Phys. Rev. Lett.* **53**, 1859 (1984).

¹¹I. G. Salisbury and M. H. Loretto, *Philos. Mag. A* **39**, 317 (1979).

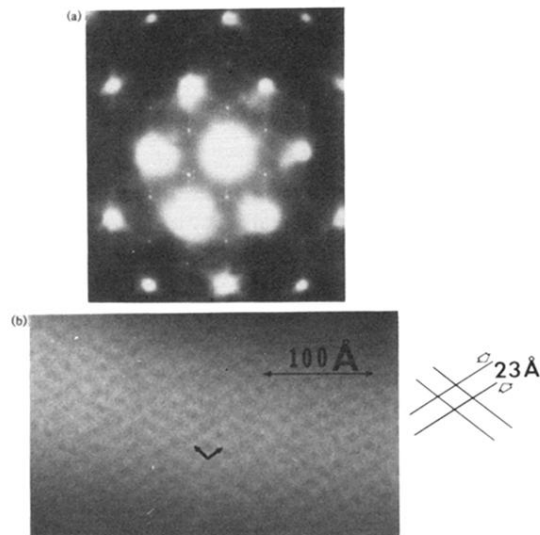


FIG. 1. (a) Transmission-electron diffraction pattern and (b) high-resolution bright-field image of the Si $\langle 111 \rangle$ (7×7) surface reconstruction in plan-view geometry from a $\langle 111 \rangle$ thin specimen. Only the $\frac{1}{7}$ th-order diffraction spots contribute to the image, giving rise to sets of 23-Å-spacing fringes. Dark areas represent regions of higher projected potential in this image.

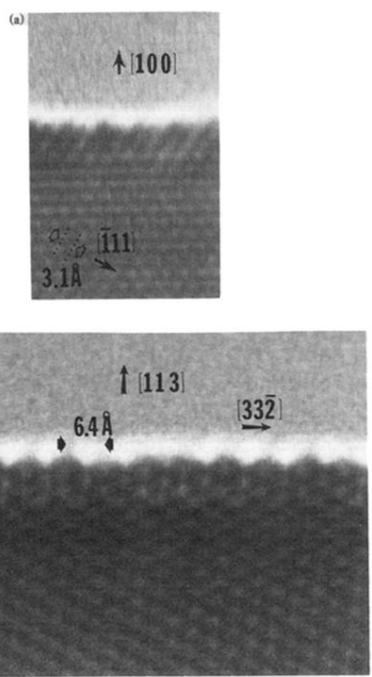


FIG. 2. Profile images at high resolution from surface facets at the edge of a $\langle 110 \rangle$ Si specimen showing (a) the $\langle 100 \rangle (2 \times 1)$ surface and (b) the $\langle 113 \rangle (1 \times 1)$ surface.